PHYSICAL REVIEW E **85**, 025303(R) (2012)

Experimental scaling law for the subcritical transition to turbulence in plane Poiseuille flow

Grégoire Lemoult,[*] Jean-Luc Aider,[†] and José Eduardo Wesfreid[‡]

Laboratoire de Physique et Mécanique des Milieux Hétérogènes (PMMH) [UMR 7636 Centre National de la Recherche Scientifique (CNRS)–École Supérieure de Physique et de Chimie Industrielles de la Ville de Paris (ESPCI)-Université Pierre et Marie Curie (UPMC)-Université Paris Diderot (UPD)], 10 rue Vauquelin, F-75005 Paris, France

(Received 8 November 2011; published 21 February 2012)

We present an experimental study of the transition to turbulence in a plane Poiseuille flow. Using a well-controlled perturbation, we analyze the flow by using extensive particle image velocimetry and flow visualization (using laser-induced fluorescence) measurements, and use the deformation of the mean velocity profile as a criterion to characterize the state of the flow. From a large parametric study, four different states are defined, depending on the values of the Reynolds number and the amplitude of the perturbation. We discuss the role of coherent structures, such as hairpin vortices, in the transition. We find that the minimal amplitude of the perturbation triggering transition scales asymptotically as Re^{-1}.

DOI: 10.1103/PhysRevE.85.025303 PACS number(s): 47.27.Cn, 47.27.De, 47.27.nd

For more than a century [1] the transition to turbulence in shear flows has been a prolific domain of study. Despite many theoretical investigations, it has not been possible to predict correctly this transitional process even for flows in simple geometries such as circular or plane Poiseuille flow (PPF) or plane Couette flow. Nowadays, the transition process in pipe and channel flows remains one of the most fundamental and practical problems still unsolved in fluid dynamics [2–4].

Linear stability theory has been applied to PPF, linearizing the Navier-Stokes equation near the stable parabolic profile. The smallest unstable or critical Reynolds number obtained was $\mathrm{Re}_c = 5772$ ($\mathrm{Re} = u_{\mathrm{cl}}h/\nu$ with u_{cl} the laminar center line velocity, h the half channel height, and ν the kinematic viscosity of the fluid) [5,6]. Carlson *et al.* [7] found $1000 < \mathrm{Re}_c < 2000$, highlighting the inadequacy of the linear stability theory to fully explain the transition to turbulence in PPF as in other shear flows.

Other approaches, related to the non-normal character of the Navier-Stokes operator linearized around the stable laminar flow solution, can support the important transient growth of finite amplitude disturbances, related to streamwise and quasistreamwise alignment [8,9].

Recently, the role of fully three-dimensional (3D), spatially extended, and coherent structures has been highlighted through numerical simulations in shear flows [10–12] and experimentally in pipe flows [13]. These traveling waves are mainly dominated by pairs of streamwise vortices associated with high and low streamwise velocity streaks.

Waleffe [14], from a 3D nonlinear modal reduction of the Navier-Stokes equations, adopted the idea of a self-sustained process as the origin of the transition. After destabilization of these streaks, streamwise modes appear and regenerate the vortices through a nonlinear interaction, as experimentally observed by Duriez *et al.* [15].

The subcritical transition to turbulence of sheared flows is characterized by an instability with respect to finite amplitude perturbation, where the larger is the Reynolds number, the smaller is the necessary perturbation. This behavior is described with a power law for the minimal amplitude of the disturbance triggering the transition:

$$\epsilon = O(\mathrm{Re}^{\gamma}).$$

After the first studies of Trefethen *et al.* [8] on the critical exponent γ, Chapman studied the transient growth of the subcritical transition process in the PPF [9]. He found $\gamma = -3/2$ for initial streamwise vortices and $\gamma = -5/4$ for initial oblique vortices.

On the other hand, the results of the nonlinear study of Waleffe and Wang show that $\gamma = -1$ in shear flows [16]. Numerical experiments of Kreiss *et al.* [17] give $-21/4 \leqslant \gamma \leqslant -1$.

Critical exponents were measured experimentally in plane Couette flow by Dauchot and Daviaud [18], in pipes by Darbyshire and Mullin [19] and Hof *et al.* [20], and in channel flow by Philip *et al.* [21]. The latter found, using a cross jet as disturbance, that the critical jet velocity triggering the appearance of hairpin vortices scales as $\mathrm{Re}^{-3/2}$.

The present Rapid Communication studies experimentally the subcritical transition of a PPF perturbed by streamwise vortices induced by jets in cross flow. We will study the transition of the Poiseuille flow using the deformation of the mean velocity profile as a criterion instead of focusing on the apparition of hairpin vortices, which is a step in the transition process.

The mean flow distortion was described in channels by Nishioka and Asai [22] and Eliahou *et al.* [23]. It is indeed now well established, that the mean flow distortion is related to the presence of streamwise and quasistreamwise elongated structures in the wall regions of boundary layers [24], pipes, and channels. These structures, alternating low and high momentum contributions to the flow, generate through a nonlinear coupling, a global modification of the flow. Recently, Barkley [25] gave a nearly complete model of the transition in pipe flow, introducing the modification of the mean velocity profile as one of the main ingredients of a system of coupled nonlinear equations.

When comparing experimental data to models, it is difficult to define properly the amplitude of the perturbation [26] and

[*]gregoire.lemoult@espci.fr
[†]jean-luc.aider@espci.fr
[‡]wesfreid@pmmh.espci.fr

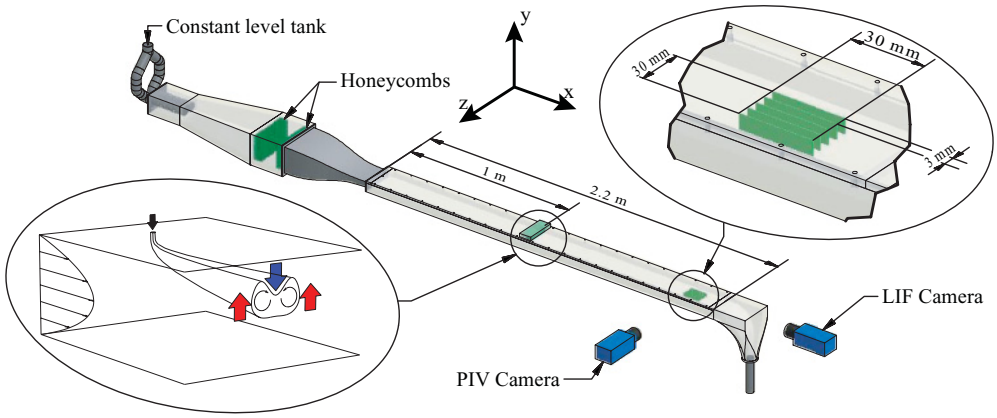

FIG. 1. (Color online) Schematic view of the dedicated water channel used at the Laboratoire de Physique et Mécanique des Milieux Hétérogènes (PMMH). The development section is 1 m long and the test section is 1.2 m long. Its cross section is 20×150 mm^2. The bottom left-hand side shows a scheme of the perturbation generation by continuous injection of water through small holes in the upper plate. The arrows represents the lift-up effect generating high- and low-speed streaks. The top right-hand side shows the scheme of the multiplane PIV technique used to compute the average velocity profile. We used 11 planes separated by 3 mm.

also its critical value triggering the transition. Our choice of selecting the mean flow distortion to characterize the transition puts special emphasis on a more rigorous definition of the onset of turbulence.

Instead of focusing on the critical value of the Re above which an initial temporally localized perturbation will develop itself spatially [27], we investigate how strong a given perturbation should be in order to sustain turbulence.

The experimental system is composed of a 3-m-long plexiglass channel (Fig. 1). The test section's half height is $h = 10$ mm, its length is $220h$, and its width is $15h$. The perturbation is generated $100h$ downstream from the inlet to ensure a fully developed Poiseuille flow for all Re. The Reynolds number is estimated from volume flow measurements. The x, y, and z axes are, respectively, the streamwise, normal to the walls, and spanwise coordinates, with $y = 0$ in the middle of the channel and $x = 0$ where perturbations are injected. The design of the inlet section, together with the smooth connections between all parts of the channel, minimize the upstream perturbations, leading to a laminar base flow until Re $= 5500$, which is the maximum Re we can reach in our setup. It has been checked that there are no sidewall effects in the central part of the channel ($-6h < z < 6h$).

The flow is perturbed by *continuous* injection of water through four circular holes, normal to the flow, drilled into the the upper wall with a diameter $d = 0.2h$ and spacing $\lambda = 3h$. The choice of a continuous perturbation, as used previously by Nishioka and Asai [22], allows us to give a description of the statistical behavior of the flow, taking into account the spatiotemporal intermittency through time averaging. The structure of the flow induced by the jets may be complex and depends strongly on the amplitude of the perturbation [28,29] defined as the velocity ratio $A = u_{\rm jet}/u_{\rm cl}$, where $u_{\rm jet}$ is the mean jet velocity and $u_{\rm cl}$ the unperturbed centerline velocity. In relation to the mass flow in the channel, our injection rate is $0.006A$. In our experiment, the injection rate varies between 0.06% and 1%. For $0 < A < 2$, one can consider that each jet creates a pair of counter-rotating streamwise vortices (Fig. 1), similar to those created by solid vortex generators in a flat-plate boundary layer [15] or in PPF [22]. Those vortices generate through a lift-up mechanism some low- and high-speed streaks elongated in the streamwise direction, similar to those naturally present in coherent structures observed in transitional flow. It has been shown that the destabilization of those streaks is a key step in a self-sustaining process between streaks and streamwise vortices in Poiseuille flow as well as in a flat-plate boundary layer [15,30]. It is also a key step in the transition scenario proposed by Chapman [9].

In Fig. 2 we show an example of visualization, obtained by laser-induced fluorescence (LIF), of the transition induced by the jets relatively far downstream from the injection. For $x < 60h$, one can see that the streamwise vortices induced by the four jets are already unstable, with clear streamwise modulation characteristic of hairpin vortices. This corresponds to the mixed behavior observed by Tasaka *et al.* [31]. The transition to turbulence occurs further downstream ($x > 60h$) over the entire channel width. In the following, all measurements will be carried on in the region $75h < x < 80h$ illustrated in Fig. 1.

The velocity field is studied by using particle image velocimetry (PIV) measurements (Figs. 1 and 3). The fluid is seeded with neutrally buoyant particles ($d_p \approx 5$ μm). To take into account the spanwise modulation of the flow, we measure velocity fields in a volume ($\Delta x = 3h$, $\Delta z = \lambda = 3h$, $\Delta y = 2h$), centered around $x = 78h$. The measurement volume is divided in 11 x-z planes between $z = \pm\lambda/2$ around a jet. For each plane, 30 instantaneous snapshots are taken at 4 Hz, giving 11 time-averaged velocity fields [Fig. 3(a)].

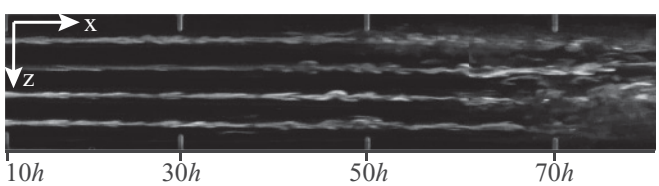

FIG. 2. LIF visualization of the transition in the $y = 0$ plane. The flow goes from the left to the right.

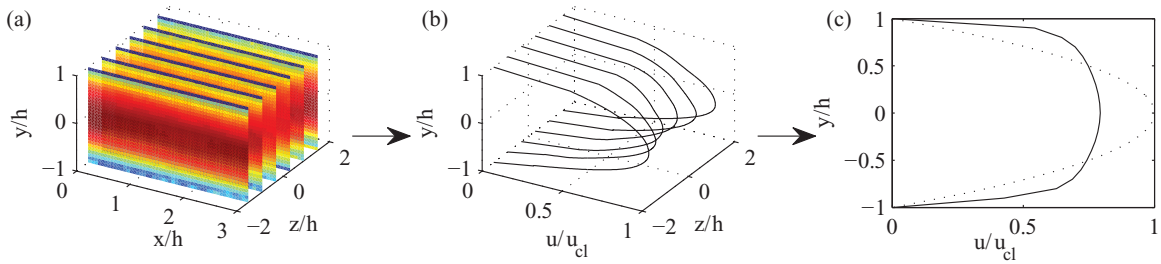

FIG. 3. (Color online) From left to right, decomposition of the steps to compute the mean velocity profile. First we measure the time-averaged (30 snapshots at 4 Hz) velocity field in 11 x-y planes (only six re apresented here), then we average in the x direction, and finally we average in the z direction.

Then the PIV fields are space averaged over the streamwise direction [Fig. 3(b)]. Finally, the 11 profiles are averaged along the spanwise direction, giving the final mean velocity profile [Fig. 3(c)]. Each mean profile presented in the following is the result of an average over 26 000 profiles. The total time to measure one mean profile is 3 min, thus averaging intermittent effects.

The transition from the laminar to the turbulent regime is associated with a deformation of the mean velocity profile from a parabolic to a plug profile (Fig. 4). The profile can then be used as a quantitative criterion to define the different states of the flow. We construct a state parameter $\tilde{u}$ as

$$\tilde{u} = \frac{\max(u)}{u_{\mathrm{cl}}},$$

where u is the perturbed mean velocity profile.

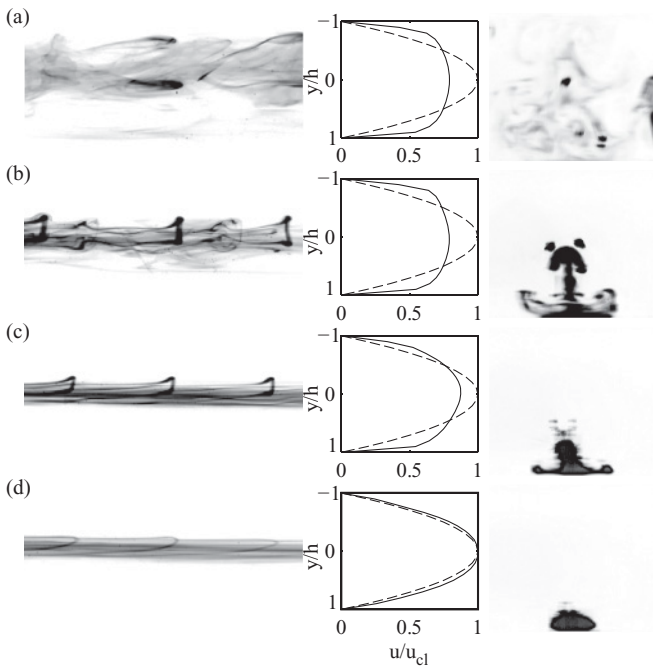

FIG. 4. The first column shows an upper side view using fluorescent dye at $x = 20h$, near the exit of the jets. The second column represent the evolution of the mean velocity profiles, measured by PIV at $x = 80h$, from which the parameter $\tilde{u}$ is defined. The third column shows snapshots taken using the LIF technique in the $x = 80h$ cross section, far from the perturbation. From top to bottom, the rows correspond, respectively, to $A = 0.276$, 0.248, 0.209, and 0.167. Re is 2830 for all rows.

In Fig. 5 we plot the evolution of $\tilde{u}$ as a function of Re ($500 < \mathrm{Re} < 5300$) and A ($0 < A < 2$). The state plane is sampled with 450 points. The sampling has been refined in the transition region. Two different domains or plateaus can be clearly identified: the laminar (red) and turbulent (blue) state, separated by a sharp cliff, giving a description of the global state of the flow. We now need to define a rigorous criterion to identify the transition.

For this purpose, fluorescent dye is added to the water tank used to feed the perturbing jets. Typical visualizations of the perturbations at $x = 20h$, near the exit of the jets, are shown in the first column of Fig. 4. In addition, we use LIF to visualize the dispersion of the tracer by using a laser sheet in the $x = 80h$ plane, far from the perturbation (third column in Fig. 2). The structure of the flow is clearly modified when the amplitude of perturbation is increased. It is illustrated in Fig. 4 for $\mathrm{Re} = 2830$. For a small perturbation (fourth row, $A = 0.167$), the flow is steady and laminar. Even if the fluorescent patches show traces of hairpin vortices, the mean velocity profile remains parabolic ($\tilde{u} = 1$). As the amplitude of the perturbation is increased (third row, $A = 0.209$), the hairpin vortices become larger but they are still smaller than the channel's half height and slightly unsteady. In this case the mean velocity profile becomes asymmetric and $\tilde{u}$ decreases ($\tilde{u} = 0.9$). For $A = 0.248$ (second row), the hairpin vortices become unstable, with intermittent excursions in the lower half of the channel. The velocity profile becomes flatter, more symmetric, and $\tilde{u}$ still decreases ($\tilde{u} = 0.82$). Finally,

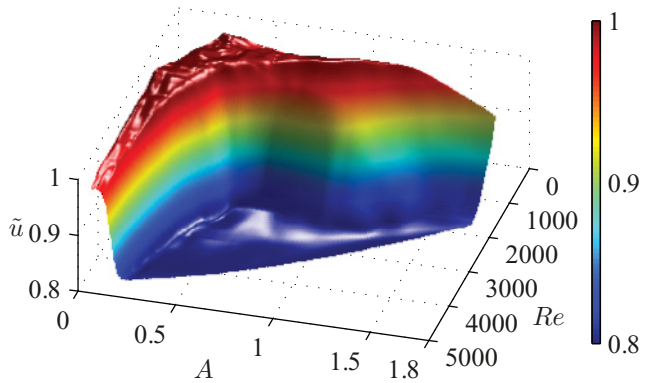

FIG. 5. (Color) 3D plot of the surface representing the parameter $\tilde{u} = \max(u)/u_{cl}$ as a function of Re and A showing well-separated domains of each state: laminar and turbulent.

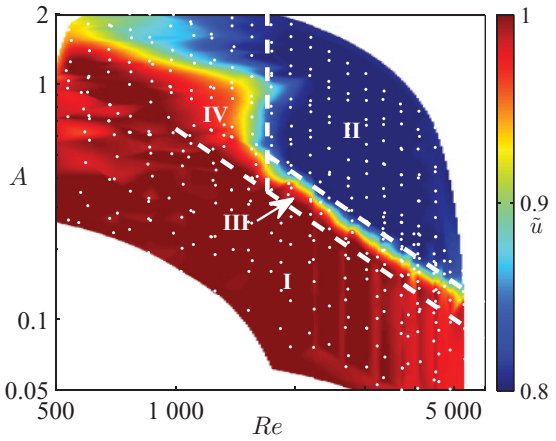

FIG. 6. (Color) Contour plot in log-log scale of $\tilde{u}(\mathrm{Re}, A)$ showing the power law for the onset of turbulence for $\mathrm{Re} > 1500$. I: Laminar state. II: Turbulent state. III: Regime dominated by hairpin vortices. IV: Below $\mathrm{Re} = 1500$ it is not possible to sustain turbulence by this means.

for $A = 0.276$ (first row), the flow becomes turbulent with large mixing over the entire cross section, leading to a typical turbulent plug profile ($\tilde{u} = 0.8$).

Owing to this analysis, it is now possible to define a quantitative criterion for the onset of turbulence. In the following, we will consider that the flow becomes turbulent when $\tilde{u} \approx 0.8$. For $0.8 \lesssim \tilde{u} < 1$, the flow is in an intermediate state dominated by hairpin vortices.

In Fig. 6 we plot the state diagram of the flow, $\tilde{u}(\mathrm{Re}, A)$, as a contour plot in a log-log representation. We define four different regions representing different states of the flow. In region I, $\tilde{u} = 1$, the flow is steady and the mean velocity profile is parabolic. This region corresponds to the laminar state. Region II ($\tilde{u} \approx 0.8$) corresponds to the turbulent state, with high mixing and a plug velocity profile. Region III ($0.8 \lesssim \tilde{u} < 1$) corresponds to a narrow intermediate state dominated by stable hairpin vortices, similar to those observed in jets in cross flow in a laminar boundary layer [29]. In region IV, perturbations induced by continuous jets do not trigger the transition, but we observe some long-lived flows different from the well-known parabolic profile.

For $\mathrm{Re} > 1500$, we define the transition line as the separation between regions II and III, corresponding to $\tilde{u} = 0.81$.

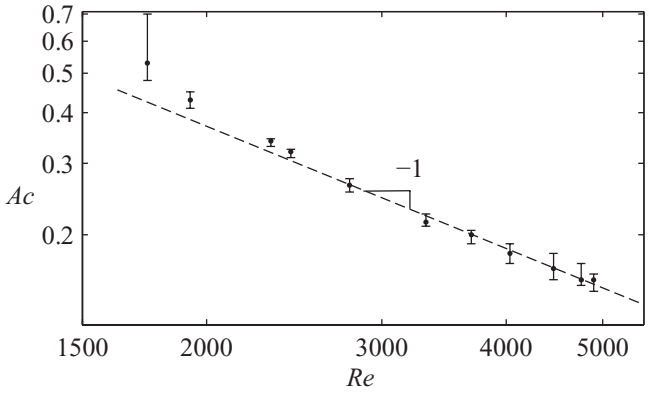

FIG. 7. Log-log plot of the stability curve for the onset of turbulence in PPF. The points correspond to $\tilde{u} = 0.81$ and the solid line is the -1 slope. The minimal amplitude triggering the transition scales as Re^{-1} for $\mathrm{Re} > 2000$.

In Fig. 7 we show a log-log plot of the minimal amplitude of the perturbation $A_c = (u_{\mathrm{jet}}/u_{\mathrm{cl}})_c = f(\mathrm{Re})$ triggering the transition, defined as $\tilde{u}(A_c) = 0.81$. The -1 slope proposed by Waleffe is added on the plot, showing good agreement for $\mathrm{Re} > 2000$. For $\mathrm{Re} < 2000$, the asymptotic regime is not reached and experimental points deviate from the -1 slope. Evaluating γ in a restricted range $1000 < \mathrm{Re} < 2000$ leads to an underestimated value for the exponent close to $\gamma = -3/2$ as found by Philip *et al.* [21].

The subcritical transition of PPF has been studied quantitatively through extensive PIV and LIF measurements. A well-defined state variable $\tilde{u}$ has been introduced. Owing to a large number of $\tilde{u}$ measurements, we could define four different regimes of the flow. We then focused on the minimal amplitude of the perturbation, A_c, triggering the transition. We found that $A_c(\mathrm{Re})$ scales as Re^{-1}, in agreement with the asymptotic nonlinear theoretical model proposed by Waleffe and Wang [16] for shear flows. Also, we contribute to develop unique ways of experimental investigation to one of the most fundamental problem in fluid dynamics.

The authors would like to thank the DGA for its support, and Dwight Barkley and Laurette Tuckerman for helpful discussions.

[1] O. Reynolds, Proc. R. Soc. London **35**, 84 (1883).
[2] S. Grossmann, Rev. Mod. Phys. **72**, 603 (2000).
[3] B. Eckhardt, Philos. Trans. R. Soc., A **367**, 449 (2009).
[4] T. Mullin, Annu. Rev. Fluid Mech. **43**, 1 (2011).
[5] C. Lin, Q. Appl. Math. **3**, 277 (1946).
[6] S. Orszag, J. Fluid Mech. **50**, 689 (1971).
[7] D. Carlson, S. Widnall, and M. Peeters, J. Fluid Mech. **121**, 487 (1982).
[8] L. Trefethen, A. Trefethen, S. Reddy, and T. Driscoll, Science **261**, 578 (1993).
[9] S. Chapman, J. Fluid Mech. **451**, 35 (2002).
[10] F. Waleffe, Phys. Fluids **15**, 1517 (2003).
[11] H. Faisst and B. Eckhardt, Phys. Rev. Lett. **91**, 224502 (2003).
[12] H. Wedin and R. Kerswell, J. Fluid Mech. **508**, 2 (2004).
[13] B. Hof, C. van Doorne, J. Westerweel, F. Nieuwstadt, H. Faisst, B. Eckhardt, H. Wedin, R. Kerswell, and F. Waleffe, Science **305**, 1594 (2004).
[14] F. Waleffe, Phys. Fluids **9**, 883 (1997).
[15] T. Duriez, J.-L. Aider, and J. E. Wesfreid, Phys. Rev. Lett. **103**, 144502 (2009).
[16] F. Waleffe and J. Wang, in *IUTAM Symposium on Laminar-Turbulent Transition and Finite Amplitude Solutions* (Springer, Berlin, 2005), pp. 85–106.

[17] G. Kreiss, A. Lundbladh, and D. Henningson, J. Fluid Mech. **270**, 175 (1994).
[18] O. Dauchot and F. Daviaud, Phys. Fluids **7**, 335 (1995).
[19] A. Darbyshire and T. Mullin, J. Fluid Mech. **289**, 83 (1995).
[20] B. Hof, A. Juel, and T. Mullin, Phys. Rev. Lett. **91**, 244502 (2003).
[21] J. Philip, A. Svizher, and J. Cohen, Phys. Rev. Lett. **98**, 154502 (2007).
[22] M. Nishioka and M. Asai, J. Fluid Mech. **150**, 441 (1985).
[23] S. Eliahou, A. Tumin, and I. Wygnanski, J. Fluid Mech. **361**, 333 (1998).
[24] T. Duriez, J.-L. Aider, and J. E. Wesfreid, ASME Conf. Proc. **2**, 791 (2006)
[25] D. Barkley, Phys. Rev. E **84**, 016309 (2011).
[26] L. N. Trefethen, S. J. Chapman, D. S. Henningson, A. Meseguer, T. Mullin, and F. T. M. Nieuwstadt, e-print arXiv:physics/0007092v1.
[27] K. Avila, D. Moxey, A. de Lozar, M. Avila, D. Barkley, and B. Hof, Science **333**, 192 (2011).
[28] A. Karagozian, Prog. Energy Combust. Sci. **36**, 531 (2010).
[29] M. Ilak, P. Schlatter, M. Bagheri, and D. Henningson (unpublished).
[30] F. Waleffe, J. Fluid Mech. **435**, 93 (2001).
[31] Y. Tasaka, T. M. Schneider, and T. Mullin, Phys. Rev. Lett. **105**, 174502 (2010).